JOURNAL OF GEOPHYSICAL RESEARCH, VOL. 105, NO. B12, PAGES 28,327-28,341, DECEMBER 10, 2000

Distribution of slip at the northern Sumatran fault system

J. F. Genrich,[1] Y. Bock,[1] R. McCaffrey,[2] L. Prawirodirdjo,[1] C. W. Stevens,[2]
S. S. O. Puntodewo,[3] C. Subarya,[3] and S. Wdowinski[4]

Abstract. We model spatial variations in horizontal displacements of 117 geodetic sites measured during annual surveys in 1989-1996 with the Global Positioning System (GPS) as elastic strain across a locked strike-slip fault to infer the contemporary slip rate, locking depth, and location of the Sumatran fault (SF) in northern Sumatra (1°S-3°N). GPS-derived slip rate estimates increase slightly northward from 23±3 mm/yr at 0.8°S to 26±2 mm/yr at 2.7°N. They agree with geologic estimates north of the equator, but at 0.5°S they are ~ 10 mm/yr higher. Strain appears to be distributed asymmetrically about the fault. South of 2°N, about 5 mm/yr of shear is required within the offshore forearc, west of the fault, to achieve a closer agreement of fault locations inferred from GPS velocities with geologically identified traces of the SF. Locking depth estimates are of the order of 10-20 km. The western branch of the major fault bifurcation near 1°N slips at a rate 5 times higher than the eastern branch. The two main strands of the fault at the northwestern tip of Sumatra (5.5°N) appear to be nearly free of horizontal strain; significant slip must occur away from the two strands, probably farther east at two other geologically active branches. The Banda Aceh embayment is extruded to the northwest at a rate of 5±2 mm/yr. Within the estimated velocity uncertainties of several millimeters per year, fault-normal deformation along the SF is insignificant. Almost strain free, the northern part of the back arc basin is part of the rigid Sunda Shelf, while the northern forearc is subjected to 8±5 x 10^{-8}yr^{-1} of extension nearly parallel to the arc.

1. Introduction

The convergent margin at Sumatra is often used as an example of partitioning of oblique plate convergence into thrust and strike-slip motions. Earthquake slip vectors along the Java trench [*McCaffrey*, 1991] and Global Positioning System (GPS) observations [*Tregoning et al.*, 1994] show that convergence between the Australian plate and the Sunda Shelf is nearly orthogonal to the trench south of Java. West of the Sunda Strait, southwest of Sumatra, slip vectors for underthrusting earthquakes at the Java trench rotate until they are oriented to the northeast (30° to 40°), suggesting that a large portion of the plate motion is taken up by right-lateral shear within the overriding plate. A simple model proposed by *Fitch* [1972] holds that the forearc plate, bounded by the trench and transcurrent fault, behaves rigidly so that long-term average slip rates can be inferred from fault geometry, slip vectors, and plate motion vectors. Such a calculation implies that there is ~ 36-49 mm/yr of dextral shear within Sumatra and the forearc region to the west [*McCaffrey et al.*, this issue]. Recent kinematic studies of the region, however, render a rigid forearc inconsistent with the slip vectors, the subduction west of the Andaman Sea, and with the observed difference of extension rates in the Sunda Strait and the Andaman Sea [*McCaffrey*, 1991; *Diament et al.*, 1992].

Here we test these ideas of slip partitioning and forearc deformation by measuring the variation in slip rates along the Sumatran fault (SF) with GPS. We initiated GPS geodetic observations in Java and Sumatra in 1989 [*Bock et al.*, 1990; *McCaffrey et al.*, 1990] as the first step in a survey of the entire Indonesian archipelago [*Puntodewo et al.*, 1994; *Tregoning et al.*, 1994; *Genrich et al.*, 1996; *Prawirodirdjo et al.*, 1997; *Stevens et al.*, 1999]. In this study, we make use of horizontal velocities of 117 geodetic sites estimated from GPS observations collected during annual surveys in Sumatra and Java in 1989-1996. These observations include multiday surveys of regionally distributed sites, including sites on the Mentawai Islands on the forearc to the west of Sumatra (Figure 1) and single-day surveys of five relatively narrow-aperture linear arrays spanning the SF (Figures 2-5). We discuss our results in the context of a comprehensive geological study of the SF by *Sieh and Natawidjaja* [this issue] and numerical models of slip partitioning and oblique plate convergence based on earthquake slip vectors and our GPS observations by *McCaffrey et al.* [this issue]. Another study by *Prawirodirdjo et al.* [this issue] discusses longer-term (~100 year) deformation from triangulation and our GPS surveys. Throughout this paper we adopt the new naming conventions suggested by *Sieh and Natawidjaja* [this issue] for different segments of the SF. We refer to the main strand of active fault segments that parallel the length of Sumatra as the "Sumatran fault" and to the SF and related structures (e.g., the Batee and Mentawai faults) as the "Sumatran fault system" (SFS).

[1]Cecil H. and Ida M. Green Institute of Geophysics and Planetary Physics, Scripps Institution of Oceanography, La Jolla, California.
[2]Department of Earth and Environmental Sciences, Rensselaer Polytechnic Institute, Troy, New York.
[3]National Coordination Agency for Surveying and Mapping, Cibinong, Indonesia.
[4]Department of Geophysics and Planetary Sciences, Tel Aviv University, Ramat Aviv, Israel.

Paper number 2000JB900158.
0148-0227/00/2000JB900158$09.00

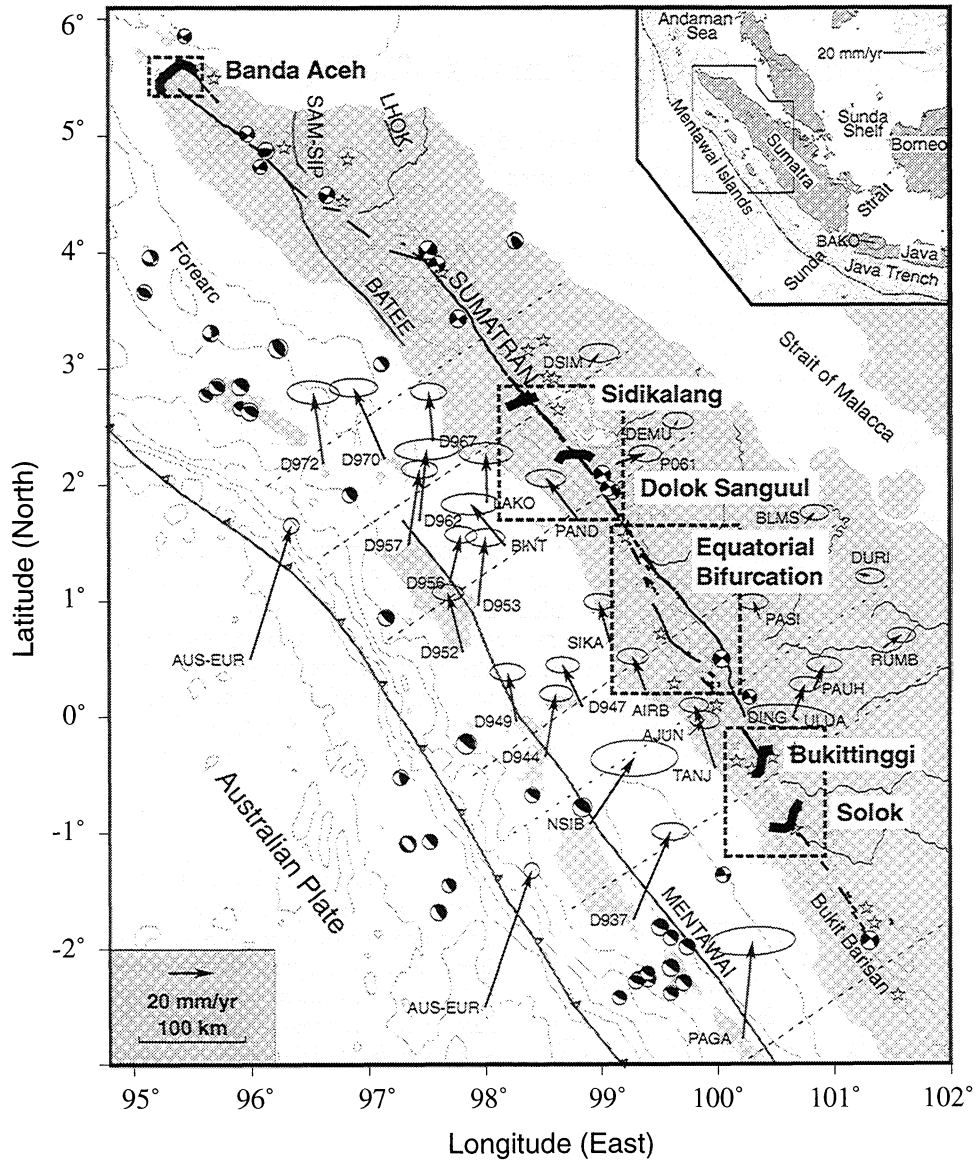

Figure 1. Index map with locations of five small-aperture arrays (labeled in bold letters) across the Sumatran fault surveyed with the Global Positioning System (GPS) in 1990-1996. The area of study is outlined on the Southeast Asia insert. Arrows represent horizontal velocities of regional stations surveyed in 1989-*1994* [*Prawirodirdjo et al.*, 1997] relative to Eurasia. Ellipses indicate 95% confidence level assuming normal distributions and a white noise model [*Zhang et al.*, 1997]. Each site is identified by a four-character code. One site on Java (BAKO) falls outside the map boundaries and is included on the insert. Arrows labeled AUS-EUR present the NUVEL-1A Australia-Eurasia relative plate motion [*DeMets et al.*, 1994]. Horizontal motion of transect and nearby regional sites located within the four rectangles outlined by thick dashed borders are the subject of subsequent figures. To model fault slip, the survey area is divided into six fault-orthogonal regions. Thin dashed lines mark the northwest and southeast margins of each region. Single width solid lines trace major rivers, bold solid lines identify faults. The Sumatran fault trace is based on data provided by K. Sieh and D. Natawidjaja. Traces of the Lhokseumawe (LHOK) and Samalanga-Sipopok (SAM-SIP) faults are simplified from *Keats et al.* [1981] and *Cameron et al.* [1983]; approximate locations of the Mentawai fault are taken from *Diament et al.* [1992]. Sketches of the onshore segment of the Batee fault follow *Cameron et al.* [1982, 1983]. Barbs indicate the margin of the overriding plate at the trench; stars indicate the location of volcanoes. Topography and bathymetry, contoured at 1-km intervals, are based on work by *Smith and Sandwell* [1997]. Focal mechanisms at the corresponding epicenters of recent (1977-1999) moderate and larger (M_w>5) shallow (<100 km) events from the Harvard centroid moment tensor (CMT) catalog [*Dziewonski et al.*, 1981] are included.

2. Regional Tectonic Setting

The main structures of Sumatra trend northwest and comprise, from southwest to northeast, the Java (Sunda) trench, the forearc ridge, the forearc basin, the Bukit Barisan mountain chain with an active volcanic arc, and finally a Neogene foreland basin that covers most of northeast Sumatra [*Hamilton*, 1979]. The most obvious shear zone within the overriding plate is the SF, located within the Bukit Barisan. It extends parallel to the trench and the volcanic chain, through

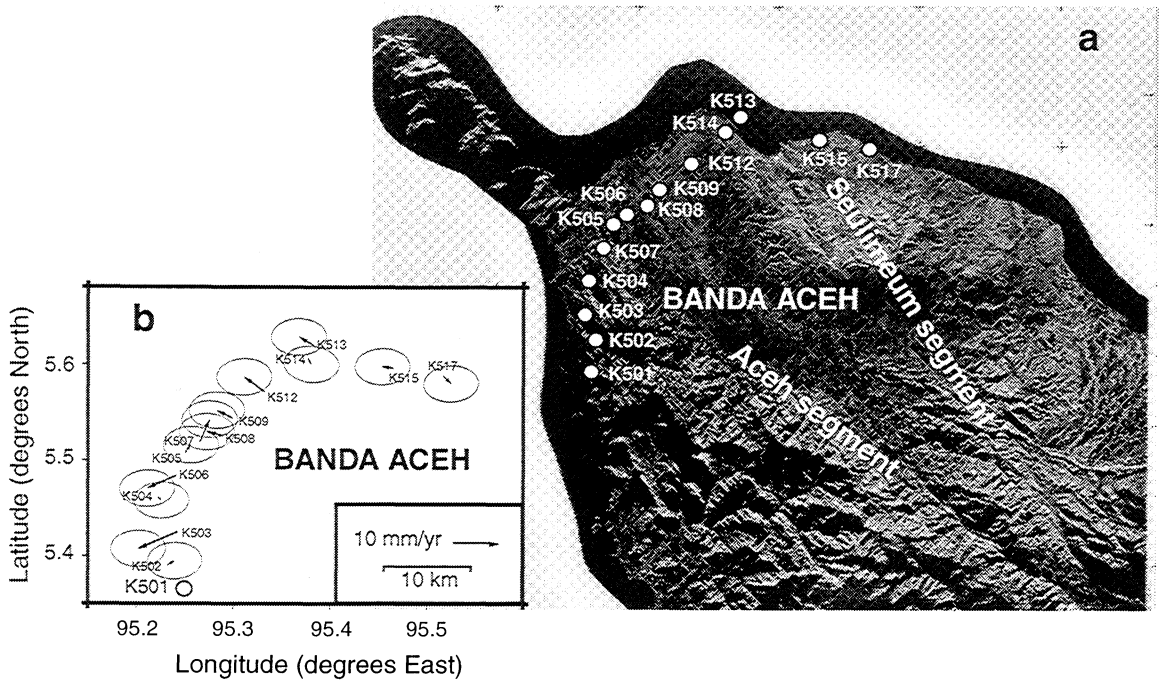

Figure 2. (a) Airborne radar image of the Banda Aceh region showing the Aceh and Seulimeum fault segments and the 14 Banda Aceh transect sites surveyed in 1992 (days 251-252), 1993 (273-274), and 1994 (268-269). (b) Horizontal velocities of geodetic sites with corresponding 95% confidence levels are shown relative to the southwesternmost station K501.

the western portion of Sumatra, for more than 1600 km along the entire length of the island from the Sunda Strait in the south to the Andaman Sea in the north. Geologic and geophysical evidence identifies the SF as a seismically active, right-lateral strike-slip fault. The SF is thought to accommodate most of the right-lateral component of the relative motion between the Australia and Eurasia plates. Roughly parallel to the direction of the trench, the orientation of major fault segments, separated by small, mostly right step overs, is fairly constant at an azimuth of N33±2°W from 2°S to the equator and beyond a major fault bifurcation at 1°N up to 2°N. Trench orientation near 2°N changes significantly, and SF strike becomes N40±2°W from 2°N to 3°N. At the northwestern tip of Sumatra (5.5°N) (Figure 2) the seismically and geothermally active Seulimeum segment strikes at an azimuth of not larger than N31°W.

The SF geologic trace is flanked by numerous volcanic edifices of mostly circular shape (see Figure 10 of *Sieh and Natawidjaja* [this issue]). The dominant exception is the large Quaternary caldera of Lake Toba (Figure 3), believed to be a complex of four overlapping parallel calderas, the youngest of which envelops the older three [*Chesner et al.*, 1991]. The major axis of the lake parallels the strike of the SF along this part of the fault. South of Lake Toba, the volcanic chain trends northward away from the SF. Together with several significant volcanic structures north of the lake, it causes a widening of the Barisan range and encloses a large oval-shaped region of elevated terrain (> 1000 m) with the Toba caldera located near the center. *Van Bemmelen* [1970] referred to this feature as the Batak tumor. The change in trend of the volcanic arc near Toba can be explained by the local geometry of the descending oceanic slab [*Page et al.*, 1979; *Fauzi et al.*, 1996; *Sieh and Natawidjaja*, this issue].

In the past 30 years, the SFS has produced more than 20 m_b>5 (or equivalently M_w>5.1 after conversion with the empirical relations derived by *Sun and Pan* [1995] for Sumatra) shallow earthquakes along its entire length [*Sukmono et al.*, 1997]. On the basis of waveform modeling of 14 m_b>5 earthquakes in 1964-1988, *Zwick and McCaffrey* [1991] arrive at a seismically determined slip rate of 1.3±0.2 mm/yr, much lower than the slip rate predicted by plate motion models, indicating that the SF, like the San Andreas fault in California, produces much less seismic moment than expected on decadal time scales. Several larger, damaging events (M_w>7) occurred on the SF within this century [*Katili and Hehuwat*, 1967; *Newcomb and McCann*, 1987]. *Prawirodirdjo et al.'s* [this issue] analysis of GPS and triangulation data over the last century suggests that the sizes of these larger earthquakes have been significantly underestimated.

Although the SF comprises a single strand in most places, it includes significant bends (Figure 4) and step overs (Figure 5) that probably control some rupture kinematics [*Sieh and Natawidjaja*, this issue]. *Bellier et al.* [1997] infer a northward increase of seismic hazard along the SFS with recurrence intervals of 400±200 years for a maximum expected M_w=7.2 event in southern Sumatra and of 160±80 yr for a M_w =7.7 maximum expected earthquake at 2°N. Very large events (M_w>8) in Sumatra are primarily associated with the subduction zone [*Newcomb and McCann*, 1987], with a recurrence time estimated at more than 100 years [*Sun and Pan*, 1995; *Zachariasen*, 1998; *Zachariasen et al.*, 1999].

3. Slip Rates

McCaffrey [1991] suggested that rotation of earthquake slip vectors and an increase in convergence obliquity toward the northwest imply an increase in slip rate along strike and arc-parallel stretching of the forearc. To match the slip vec-

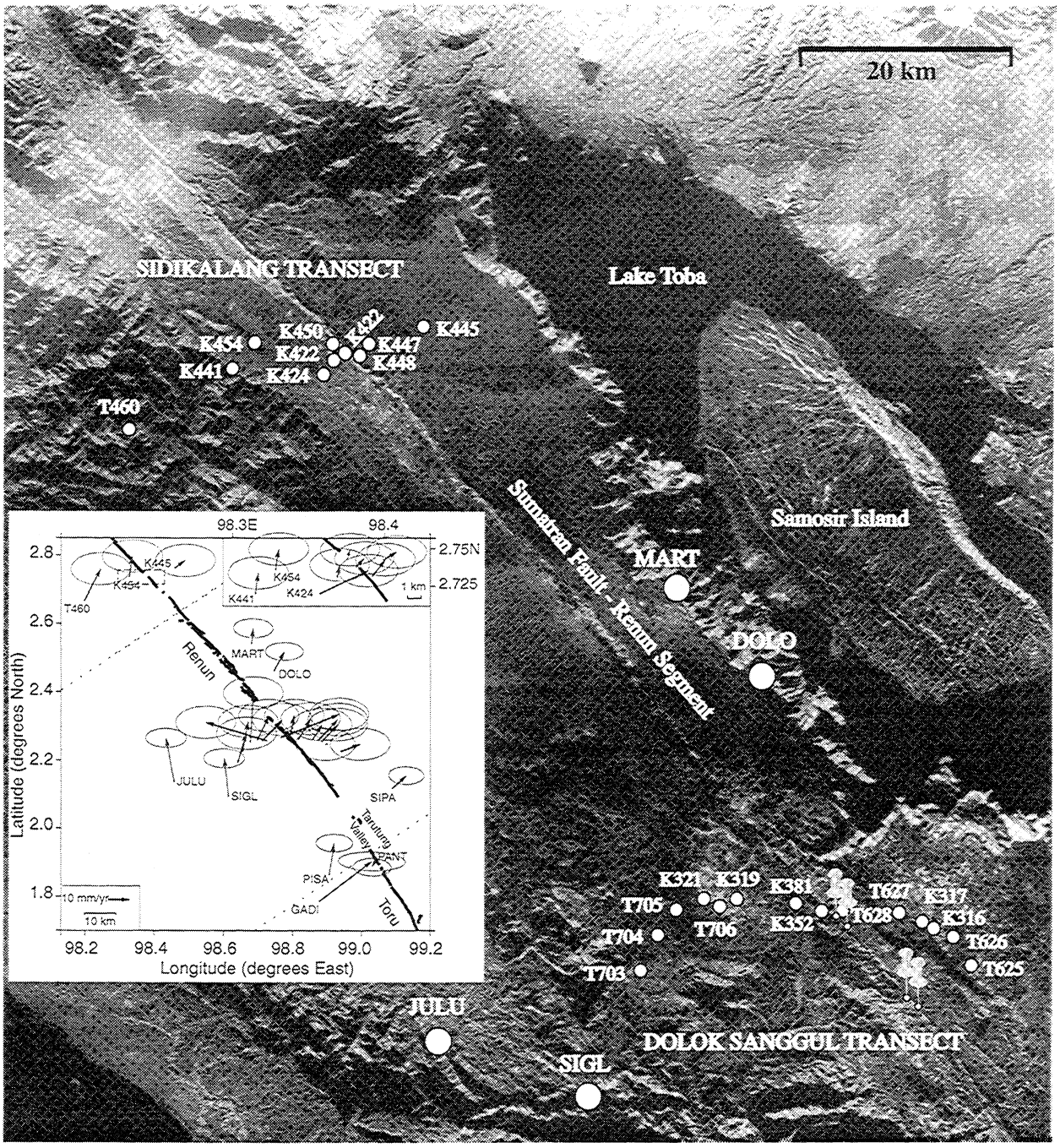

Figure 3. Airborne radar image of the Lake Toba region with a clear delineation of the trace of the Sumatran fault. Included are the regional GPS sites (large white dots) and the sites of the Sidikalang and Dolok Sanggul transects (small white dots) measured in 1991-1994 and in 1996. The push pins locate two recognizable ~2 km offsets of the 73,000-year-old Toba tuff, which have been used to determine a 28 mm/yr geologic slip rate of the fault by *Sieh et al.* [1991]. Inset shows horizontal site velocities of transect sites and nearby regional stations with respect to Eurasia. Top right corner plot of inset shows velocity arrows of near-fault Sidikalang transect sites located within the dashed rectangle. Station K454 is also included in the main plot for orientation.

tors the arc-parallel forearc stretching rate needed is 2-3 x 10^{-8} yr^{-1}, and slip rate along the SFS could increase from zero near the Sunda Strait to a maximum of 45-60 mm/yr near the Andaman Sea. For the northern Sumatra region between 2°S and 3°N *McCaffrey et al.* [this issue] found that slip vectors reveal arc-parallel velocities of 23-27 mm/yr.

From offsets in late Quaternary tuff deposits, *Sieh et al.* [1991, 1994] estimated geological slip rates along the central part of the SF ranging from 11 to 28 mm/yr (Table 1, see also Figure 3). *Bellier and Sébrier* [1995] analyzed stream offsets on SPOT images to infer slip rates at several locations along the fault. Their rates range from 6±4 mm/yr at 5°S to 23±2 mm/yr at 2°N, but the underlying estimates of elapsed time often lack specific dating of the involved geologic units. The overall increase in dextral motion of ~ 18 mm/yr between 5°S and 2°N, however, is less than the expected rate differ-

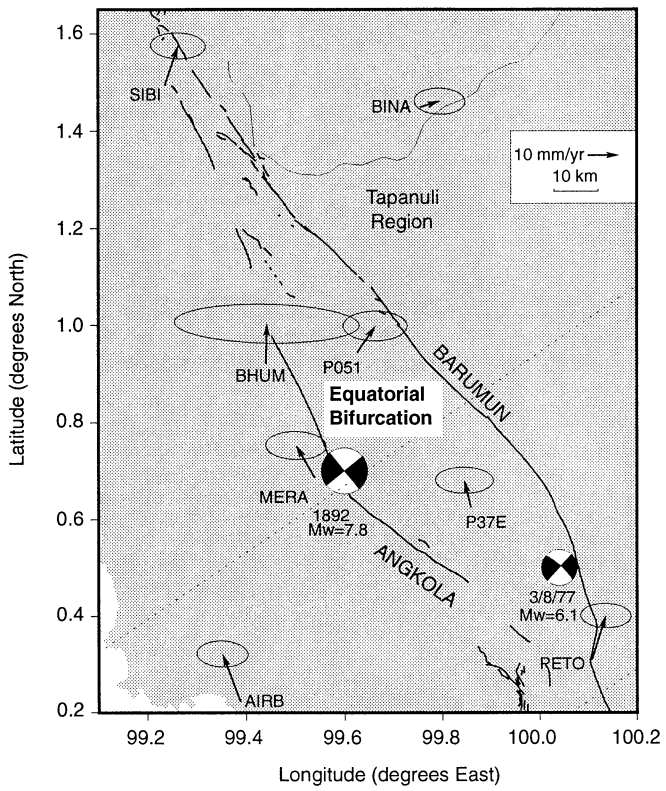

Figure 4. The region of the equatorial bifurcation in the Sumatran fault near 1°N. Shown are horizontal velocities of regional stations and corresponding 95% confidence levels with respect to Eurasia. Epicenter and focal mechanism of the most recent moderate earthquake in the region, on March 8, 1977, are taken from the Harvard CMT catalog; approximate parameters for the 1892 event are based on work by *Prawirodirdjo et al.* [this issue].

ence of 30 mm/yr that *Bellier and Sébrier* [1995] inferred from opening rates of marginal oceans at the southern and northern ends of Sumatra (Sunda Strait and Andaman Sea).

4. GPS Surveys

Field observations for a 5-year GPS project in Sumatra, GPS Geodynamics Project in Sumatra (GPS-GPS), started in 1989 with a 33-station deployment, mostly in the Indonesian provinces of north and west Sumatra. For historical, logistical, and budgetary reasons we made use of several types of existing monuments. The first type, primarily located on the remote Mentawai Islands, were geodetic pillars constructed for a joint Indonesian-Australian Doppler (TRANSIT satellite) survey carried out in the early 1980s. The second type, located on the mainland and mostly on remote mountaintops, were triangulation pillars constructed by Dutch and Indonesian surveyors near the turn of the century [*Prawirodirdjo et al.*, this issue]. Finally, for the remainder of the sites, new monuments were constructed consisting of steel pipes anchored in square-shaped concrete blocks equipped with a brass plate or stainless steel pin to serve as the survey mark. In subsequent years the regional network was expanded to include more than 50 sites.

The initial campaign in 1989 was plagued by a sparse GPS satellite geometry in the Sumatra region and intense ionospheric activity that caused about half of our GPS receivers to lose the ability to track the L2 carrier signal. Nevertheless, we were able to obtain good dual-frequency data from the remaining (TI-4100) GPS receivers. In 1990 the combined adverse effects of GPS selective availability (SA) and unsynchronized global tracking [*Feigl et al.*, 1991] reduced geodetic precision compared to surveys in subsequent years. These later surveys also benefited from improved receiver technology, increasingly favorable satellite constellation, and the establishment of the International GPS Service in 1992 with a robust global GPS tracking network [*Beutler et al.*, 1993]. Locations on Sumatra were typically observed four times (1989, 1990, 1991, and 1993), while most forearc sites (Mentawai Islands) were occupied at 2-year intervals (1989, 1991, and 1993). Data from key reference stations BAKO (west Java, Figure 1), MART (Figure 3), and PADA (Figure 5) were collected during all five annual surveys and in 1996. During each annual survey each regional site was occupied for an average of four consecutive days with 12 to 22 hours of continuous daily observations each day.

To measure the near-fault strain field along the SF, we established, in connection with our annual regional GPS surveys in Sumatra, five short, near-linear, fault-crossing arrays (transects) of 9 to 15 stations each (Figure 1). The arrays incorporate existing leveling monuments spaced at intervals of ~ 5 km along paved, fault-crossing roads. The arrays were densified by constructing new points between the leveling sites. The transects are named after the towns situated near

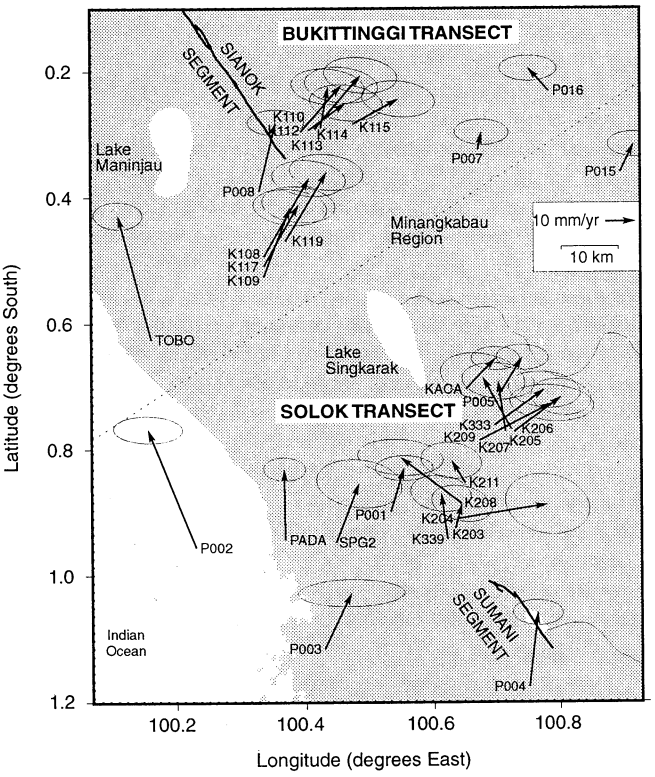

Figure 5. Horizontal site velocities of Solok and Bukittinggi transects and nearby regional stations with respect to Eurasia. These transects were surveyed in 1990 (days 197-200), 1991 (166-168), 1992 (242-244), 1993 (242-244), and 1996 (259-261). The bold solid line segments of the mapped Sumatran fault trace suggest a step over in this area [*Sieh and Natawidjaja*, this issue].

Table 1. Geologic Estimates of Sumatran Fault Dextral Slip Rates

Latitude	Slip Rate, mm/yr	Reference	Type of Observed Offsets
0-3.5°S	11	*Sieh et al.* [1994]	late Quaternary volcanic units
0.5°S	12	*Natawidjaja and Sieh* [1994]	Maninjau Tuff
1.6°N	10	J. Dobson (Unocal Geothermal, personal communication, 1999)	Quaternary deposits
2°N	23±2	*Bellier and Sébrier* [1995]	SPOT images
2.2°N	28	*Sieh et al.* [1991]	Toba Tuff
5°N	38±4	inferred from data by *Bennett et al.* [1981a]	Quaternary deposits

their centers. The two southernmost (Solok and Bukittinggi) are located just south of the equator in the Minangkabau area of west Sumatra (Figure 5), two span the fault near the northern (Sidikalang) and southern shores (Dolok Sanggul) of Lake Toba (Figure 3), and the fifth covers the northern tip of Sumatra near Banda Aceh (Figure 2).

Observations on the transects were initiated in 1990 at several sites along the Minangkabau and southern Lake Toba transects. Because of the effects of SA and a relatively short observation span the 1990 measurements did not achieve the necessary accuracy of a few millimeters. Observations (single- or double-day at 7-12 hours per day) in subsequent years (1991-1994, 1996) were considerably more accurate. Concurrent measurements at several regional sites (PADA, SPG2, MART, P54E) tied the transects to the regional network. The Banda Aceh transect was established and first surveyed in 1992. Resurveys of 14 stations followed in 1993 and 1994. Since no regional sites were operated concurrently during these resurveys and since the observation period of 8-10 hours was too short to permit an accurate tie to any global fiducial station or network, our displacement field for the Banda Aceh array is only local, that is, we can only calculate relative displacement between sites of the array.

5. GPS Data Processing

GPS data analysis for the subset of regional stations follows the method summarized by *Prawirodirdjo et al.* [1997] and detailed by *Bock* [1998]. Dual-frequency carrier phase and pseudorange observations of 58 regional stations and transect sites are combined with orbital parameters calculated from a network of global reference sites to yield daily estimates of station coordinates, tropospheric zenith delay parameters, and phase ambiguities by weighted least squares adjustment. Daily solutions for the early GPS campaigns (prior to 1992) included observations from all available global tracking stations (10 in the Northern Hemisphere plus Wellington, New Zealand, and the Australian sites at Canberra, Hobart, and Townsville). Starting in 1992, we selected only global reference sites with mutual satellite visibility with the regional network. These stations (Kokee and Pamate in the Pacific, Yaragadee and Canberra in Australia, McMurdo in Antarctica, and Taipei and Usuda in Asia) were also part of a daily global solution for the computation of the GPS satellite orbits, Earth orientation parameters, and station coordinates [*Fang and Bock*, 1995, 1996]. A Kalman filter algorithm [*Herring*, 1997] merges the sequence of daily solutions with corresponding estimates of the reference frame (coordinates of global tracking sites, satellite state vectors, and Earth orientation parameters) to obtain station coordinate and velocity estimates in the International Terrestrial Reference Frame (ITRF96) [*Sillard et al.*, 1998]. Finally, we employ the Eurasia - No Net Rotation (EUR-NNR) NUVEL-1A Euler pole (50.6°N, -112.4°E, 0.229°/Ma) [*Argus and Gordon*, 1991; *DeMets et al.*, 1994] to convert to station velocities relative to Eurasia.

North velocity components have typical formal one standard deviations (assuming a white noise stochastic model for the estimated site coordinates [see *Zhang et al.*, 1997]) of 2 mm/yr (regional) and 3-4 mm/yr (transect); east components have standard deviations of 4 and 5-7 mm/yr, respectively (Table 2). Figure 1 presents the broad-scale velocity field derived from our GPS data. Figures 2-5 show the detailed, near-field velocities at various locations along the SF (north to south), including velocities derived from the dense fault-crossing GPS arrays.

6. GPS Survey Results

6.1. Back Arc Basin

The velocity field in Figure 1, plotted relative to a stationary Eurasia plate, clearly shows right-lateral motion across the SF. Velocities (Table 2) of stations located in the central Sumatra back arc basin (RUMB, DURI, BLMS, DEMU, and DSIM) suggest that the relative motion of this region is small (6±4 mm/yr) with respect to Eurasia. A similar observation holds for GPS-measured sites on Java, Bali, Borneo, and Sulawesi [*Genrich et al.*, 1996]. Five stations on these islands define a Sunda Shelf (SSH) rigid tectonic area that rotates at 0.38±0.05°/Myr relative to the no-net-rotation (NNR) reference frame with a pole at (54±5°N, -155±15°E). Expanding the SSH to include the central Sumatra basin, adding additional sites from the other islands, but excluding one site in southeastern Sulawesi, yields a SSH-NNR pole of (49±5°N, -100±7°E, 0.28±0.05°/Myr) with a χ^2 of 0.92 per degree of freedom for a total of 15 sites. The good fit and the moderate size of weighted residuals for the Sumatra stations confirm that the Sumatra back arc forms part of the Sunda Shelf. The formal uncertainties of the parameter estimates are too large to consider this pole significantly different from the NUVEL-1A EUR-NNR pole. A statistical F-test on corresponding χ^2 values, however, reveals a significantly better fit of the GPS-measured velocities at the 15 sites to the SSH pole, suggesting that SSH kinematics are different from those of Eurasia.

Table 2. Station Coordinates (WGS84) and Horizontal Components of Displacement Rates Relative to Eurasia[a]

Site Code	Lon., °E	Lat., °N	Height, m	North, mm/yr	East, mm/yr	N-E Error Correlation
K503	95.2429	5.4250	-32	-9±6	-4±4	0.023
K504	95.2436	5.4702	-33	2±6	-1±4	0.025
K501[a]	95.2501	5.3645	-31	0	0	0
K502	95.2531	5.3987	-31	3±6	2±4	0.029
K506	95.2621	5.4928	-33	-13±6	-6±4	0.024
K505	95.2716	5.5167	-32	3±6	4±4	0.029
K507	95.2868	5.5281	-31	4±6	10±4	0.028
K508	95.3084	5.5356	-31	-6±6	1±4	0.028
K509	95.3206	5.5535	-30	-7±6	3±4	0.022
K512	95.3537	5.5811	-32	-9±6	7±4	0.025
K514	95.3985	5.6162	-33	2±6	-3±4	-0.065
K513	95.4046	5.6298	-33	-7±6	4±4	0.023
K515	95.4873	5.6058	-2	-5±6	1±4	0.026
K517	95.5394	5.5976	62	4±6	-4±4	0.026
D972	96.6245	2.1890	-20	-4±7	32±3	-0.095
D970	97.1505	2.2233	-25	-14±6	33±2	0.004
D957	97.3508	1.4877	-20	5±5	34±2	-0.058
D962	97.4465	1.6974	-21	3±8	32±3	0.106
D967	97.5626	2.3796	-24	-2±5	22±2	-0.055
D956	97.7060	1.1658	-14	5±4	22±2	-0.054
D952	97.8185	0.5625	19	-7±4	27±2	-0.057
D953	97.9456	0.9647	-17	3±5	31±2	0.065
LAKO	98.0254	1.8454	-17	0±7	23±3	-0.027
BINT	98.1779	1.4787	-16	-16±6	19±2	0.013
T460	98.1980	2.6650	402	8±7	16±4	0.018
D949	98.2744	-0.0355	-14	-4±5	22±2	-0.036
K441	98.3149	2.7199	1087	1±7	10±4	0.018
K454	98.3281	2.7357	1085	2±7	10±4	0.020
K424	98.3569	2.7200	1145	24±7	11±4	0.027
K422	98.3686	2.7309	1094	1±7	6±4	0.018
K450	98.3753	2.7429	1023	1±7	5±4	0.034
K442	98.3810	2.7377	965	4±7	4±4	0.019
K448	98.3917	2.7316	879	7±7	8±4	0.015
K447	98.3989	2.7424	1008	7±7	4±4	0.017
JULU	98.4588	2.1362	488	-4±5	21±2	-0.021
K445	98.4592	2.7621	1380	5±7	4±4	0.018
D944	98.5261	-0.3429	-14	5±4	29±2	-0.003
SIGL	98.6154	2.0922	1506	-2±5	19±2	-0.014
T703	98.6418	2.1923	1303	4±7	14±4	0.018
T704	98.6563	2.2248	1409	3±7	15±4	0.018
T705	98.6778	2.2524	1465	1±7	24±4	0.021
MART	98.6823	2.5412	918	1±5	8±2	0.051
K321	98.6980	2.2595	1438	6±7	12±4	0.019
T706	98.7117	2.2568	1394	10±7	11±4	0.016
K319	98.7253	2.2575	1387	-29±7	9±4	0.023
DOLO	98.7463	2.4622	2145	5±4	9±2	-0.014
K381	98.7650	2.2667	1415	28±7	11±4	0.000
K352	98.7907	2.2620	1499	2±7	12±4	0.019
T628	98.8164	2.2614	1372	6±7	10±4	0.018
PAND	98.8188	1.6872	-10	-15±5	20±2	-0.066
D947	98.8460	0.0859	-8	-9±4	19±2	-0.054
T627	98.8593	2.2624	1403	4±7	7±4	0.020
K317	98.8737	2.2587	1403	10±7	10±4	0.019
GADI	98.8779	1.7858	1043	25±8	19±2	-0.085
K316	98.8838	2.2548	1399	8±7	8±4	0.020
T626	98.9021	2.2485	1394	-1±7	0±4	0.008
DSIM	98.9036	3.0130	1498	5±5	6±2	0.011
PISA	98.9068	1.8639	764	2±4	15±2	-0.033
NSIB	98.9094	-0.9216	-14	20±11	30±5	0.064
T625	98.9393	2.2250	1310	10±7	4±4	0.017
PANT	99.0448	1.9130	911	-2±4	-4±2	-0.058
SIKA	99.0838	0.6422	279	-5±4	19±2	-0.042
SIPA	99.0890	2.1168	1211	7±4	6±2	0.091
P061	99.1364	2.1770	1773	14±4	5±2	-0.024
BONA	99.1844	2.4646	958	45±7	-9±4	0.020
SIBI	99.2359	1.4941	869	4±4	13±2	-0.054
D937	99.2781	-1.7466	-13	17±5	40±2	-0.024
AIRB	99.3879	0.2226	246	-6±4	16±2	-0.049
BHUM	99.4409	0.9214	1234	0±15	13±3	-0.096
MERA	99.5393	0.6860	2134	-6±5	11±2	-0.038
P051	99.6261	0.9439	2005	6±5	9±2	0.002
DEMU	99.6288	2.4788	17	2±4	4±2	-0.031
BINA	99.7553	1.4489	112	6±4	2±2	-0.043
AJUN	99.7655	-0.1584	28	7±4	7±2	-0.059
P37E	99.8591	0.6245	1008	-2±5	9±2	-0.025
TANJ	99.9867	-0.4443	48	-10±4	29±2	-0.037
PETO	100.1071	0.3097	330	5±4	14±2	-0.044
TOBO	100.1628	-0.6256	29	-11±4	43±2	-0.030
PAGA	100.2150	-2.7769	-11	5±11	45±4	0.148
P002	100.2308	-0.9559	-5	-16±6	40±2	-0.048
P008	100.3311	-0.3900	2870	6±5	23±2	0.065
K109	100.3375	-0.5256	205	9±6	24±3	-0.162
K117	100.3383	-0.5090	282	12±6	21±3	-0.163
K108	100.3384	-0.4939	374	15±6	27±3	-0.162
PADA	100.3692	-0.9438	3	0±3	24±2	-0.039
PASI	100.3692	0.8439	61	-3±4	8±2	-0.042
K119	100.3716	-0.4694	618	14±6	24±3	-0.161
K110	100.3956	-0.2959	901	14±6	16±3	-0.163
K112	100.4080	-0.2934	901	13±6	9±3	0.069
K113	100.4177	-0.2912	900	16±6	18±3	-0.160
K114	100.4268	-0.2893	892	3±6	14±3	-0.158
P003	100.4293	-1.1166	871	9±9	19±2	0.043
SPG2	100.4487	-0.9483	111	8±7	20±4	-0.157
K115	100.4777	-0.2837	873	15±6	9±3	-0.159
P001	100.5337	-0.8992	1855	5±5	15±2	-0.001
K339	100.6221	-0.9435	998	-2±5	16±3	-0.157
K203	100.6345	-0.9265	875	2±5	9±3	-0.254
K204	100.6377	-0.9108	772	31±7	5±5	-0.153
K208	100.6436	-0.8859	570	-21±7	16±3	-0.149
DING	100.6538	-0.0075	1593	5±4	15±2	-0.032
K211	100.6506	-0.8543	438	-5±5	8±3	-0.153
KACA	100.6526	-0.7056	761	10±4	10±2	-0.031
P007	100.6732	-0.3245	2258	1±4	6±2	-0.036
K209	100.6736	-0.7871	392	25±7	13±3	-0.155
ULUA	100.6948	-0.0372	860	-3±11	2±3	-0.302
K333	100.6974	-0.7628	397	17±6	12±3	-0.154
P005	100.7037	-0.7159	1188	8±4	13±2	-0.037
K205	100.7148	-0.7726	351	-3±6	17±3	-0.153
K206	100.7237	-0.7689	340	-10±7	18±4	-0.246
K207	100.7284	-0.7733	331	16±5	12±3	-0.153
P004	100.7504	-1.1769	2563	3±4	25±2	-0.042
BLMS	100.7599	1.6637	15	4±4	5±2	-0.037
P016	100.7850	-0.2323	1271	-7±5	8±2	-0.006
PAUH	100.8324	0.2372	413	5±5	11±2	-0.022
P015	100.8984	-0.3612	1272	5±4	10±2	-0.038
DURI	101.2194	1.2307	39	5±4	-1±2	-0.033
RUMB	101.4341	0.5923	40	8±4	6±2	-0.039
BAKO	106.8489	-6.4911	159	7±3	-1±2	-0.029

[a]Displacement rates for Aceh transect stations (K501-K517) are relative to K501.

6.2. Banda Aceh Transect

The 41-km-wide transect spanning the two major, subparallel, seismically active SF strands (Aceh and Seulimeum segments, Figure 2) at the NW tip of Sumatra shows a total right-lateral displacement of only 5±4 mm/yr. Relative station displacements for 1993-1992 and 1994-1993 are consistent and therefore lend credibility to this velocity field that is based only on three observation periods with a total time span of 2 years. Because we do not have displacements of

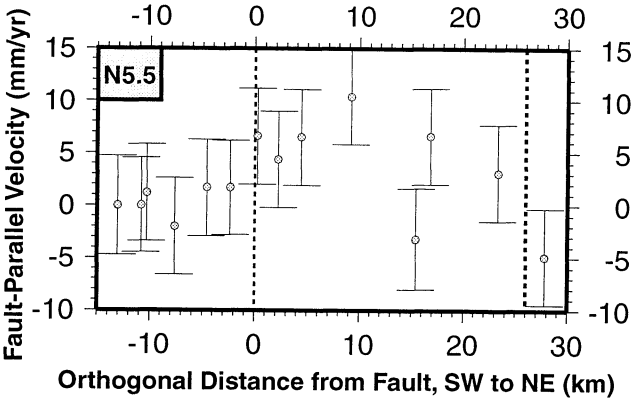

Figure 6. Fault-parallel components (circles) of GPS-measured displacement rates with associated formal one standard deviations as a function of orthogonal fault distance for the Banda Aceh transect. Site velocities are shown relative to the southwesternmost station (K501). Vertical dashed lines indicate the relative location of the main Sumatran fault strands at this latitude (5.5°N), the Aceh (taken as the reference location at the origin of the x axis) and the Seulimeum (right) segments.

the Banda Aceh sites relative to Eurasia or some other regional reference frame, we can only establish an upper bound to the slip rate at this latitude assuming that the locking depth does not exceed 15 km and that the array spans the fault. With no site velocities available in the far field, however, we cannot rule out that most of the motion occurs outside the region covered by the geodetic array. Inspection of fault-parallel rates (Figure 6) suggests relative northwestward motion of the area located between the two major fault strands. A Student's t-test [e.g., *Dowdy and Wearden*, 1991], performed on the two fault-parallel rate populations of stations inside (K507-K515) and outside (K502-K506 and K517) of this area (Figure 2), confirms that the alluvium of the Banda Aceh embayment is extruded to the northwest at a significant rate of 5±2 mm/yr.

6.3. Sidikalang and Dolok Sanggul Transects

Velocities for the Sidikalang and Dolok Sanggul transect stations near Lake Toba are shown in Figure 3 relative to stationary Eurasia. Sites JULU, SIGL, and PISA, located west of the fault, clearly show right-lateral motion. The dense fault-crossing transects, however, suggest that the right-lateral shear occurs not along the SF trace drawn on the map but at a significant distance west of it. The transects stations also appear to have a larger fault-normal component of motion than the nontransect sites, but large uncertainties prevail.

6.4. Solok and Bukittinggi Transects

Although our velocity estimates are formally based on five measurement epochs covering six years (1990-1996), they are dominated as described earlier by the three latest GPS campaigns (1992, 1993, and 1996). Geomorphologically identified segments of the SF trace meet near Lake Singkarak at a right-stepping discontinuity of several kilometers (Figure 5 [see also *Sieh and Natawidjaja,* this issue, Plate 1]. The associated spatial transfer of slip is confirmed by our geodetic observations. South of the lake (Solok transect, 0.8°S), deformation is centered about the identified fault trace (Sumani segment). To the north (Bukittinggi transect, 0.4°S), slip occurs along the southward extension of the Sianok fault segment trace. *Sieh and Natawidjaja* [this issue, Figure 7] suggest that the Singkarak graben represents a total of 23 km of offset (the length of the arcuate normal faults zones on either side of the lake), inferred from their observations of 3.5 km of dextral slip in the vicinity of the step over and a 7.5-km offset of the normal faults bounding the lake. If the currently observed slip rate of 23±3 mm/yr in that region serves as a good approximation of the average rate, Lake Singkarak may be about 1 Myr old. Some of the stations comprising the Bukittinggi and Solok transects have significant fault-normal velocity components, although, taking into account the large E-W uncertainties, the fault-normal component may not be significantly larger than those of the non-transect sites.

7. Elastic Dislocation Modeling

To estimate slip rates and locking depths at the SF, we invert the fault-parallel components of our GPS-measured velocities using a simple elastic dislocation model. *Prawirodirdjo et al.* [1997] have modeled this GPS data set (minus the transect stations) and shown that the arc-normal components are sufficiently explained by strain accumulation on the subduction interface, without any fault-normal motion at the SF. This result is corroborated by *McCaffrey et al.* [this issue], who demonstrated that the oblique Australia-Eurasia convergence is almost fully partitioned between arc-normal contraction on the forearc and arc-parallel shear strain near the SF. Furthermore, although the transect velocities at the Sidikalang, Dolok Sanggul, Bukittinggi, and Solok transects appear to have large fault-normal components, their E-W uncertainties are especially high, suggesting that the fault-normal velocity is not significantly higher than at the other (nontransect) GPS stations. For these reasons we model only the arc-parallel components of our GPS velocity field.

We model the SF as a vertical (90° dip) strike-slip fault in an elastic half-space. These assumptions of vertical fault geometry and pure strike-slip are significant simplifications but are justified by lack of conclusive evidence to the contrary. Although we recognize the SF to be segmented and wish to estimate slip rates at various locations along the fault, for simplicity, we treat the SF as an infinitely long fault (thus ignoring edge effects). We assume that most of the SF is locked from the surface down to some significant depth, as evidenced by its seismic history and surface expression [see *Sieh and Natawidjaja*, this issue]. However, on the basis of the seismic slip deficit along the SF [*Zwick and McCaffrey*, 1991], we allow for fault creep.

Having made these assumptions, we can use *Savage and Burford's* [1973] formulation for one-dimensional, fault-symmetric, surface displacement due to a locked strike-slip fault, modified to allow fault creep:

$$v(x) = (v_s - v_c)\,\pi^{-1}\arctan\left[(x-x_f)d^{-1}\right)] + 0.5\,v_c\,[H(x-x_f) - H(x_f-x)] + v_r. \quad (1)$$

Here, v is the velocity as a function of fault-orthogonal distance x. The origin of the x axis coincides with the geologic trace of the fault. The geodetic estimate of the fault location is x_f, v_s is the total (far field) slip rate, v_r is a (constant) reference velocity, and d is the locking depth. To account for fault

creep, we include a creep rate v_c. H denotes the Heaviside function ($H(x)=1$ for $x>0$, $H(x)=0$ otherwise).

Assuming constant values for v_c and for the strike angle, we employ an iterative procedure to solve for v_s, d, and x_f by Gauss-Newton method [e.g., *Hartley*, 1961]. Initial parameter values are derived from geologic (v_s=30 mm/yr, x_f=0, that is, the model fault plane is located at the geologic fault trace) and seismic (d=15 km) evidence. For each step of the iteration we linearize the model (with respect to the three parameters) by truncating a Taylor series expansion at the parameter estimates of the previous step and compute correction terms by solving the normal equations using least squares. Tests with different starting parameter values yield the same final estimates, suggesting the existence of unique solutions within the domain of physically reasonable numbers. Parameter estimates, their corresponding standard deviations, and the associated root-mean-square (RMS) data misfit converge (constant at three significant figures) after 5 to 20 iterations. We compute least squares solutions while varying creep rates in increments of 1 mm/yr and strike angles in steps of 1° from N30°W to N40°W. Uncertainties for our model parameter estimates are the standard deviations computed from the linearized problem of the last iteration steps.

To investigate relative sensitivity of the three model parameters with respect to the GPS-determined site velocities, we compute the three corresponding partial derivatives. We observe that absolute values of $\delta v/\delta v_s$ increase with distance from the fault, while the other two derivatives decrease away from the fault. Hence, assuming equal measurement errors, estimates of total slip rate depend predominately on observed far-field velocities, whereas model locking depth and fault plane location are largely determined by near-fault data. Since equation (1) is essentially a function of the normalized distance $(x-x_f)d^{-1}$, the estimates of fault plane location and locking depth are highly correlated.

The five stations of the central Sumatra basin (DSIM, DEMU, BLMS, DURI, and RUMB, Figure 1) reveal very little relative displacement, and their average fault-parallel motion is small (1±4 mm/yr) with respect to Eurasia. We therefore assume that almost all strain associated with dextral shear in the upper plate is located between the trench and the basin. Our reference velocity is then determined by the convenient choice of a vanishing slip rate at large positive x values. Evaluating equation (1) at $x = \infty$ yields $v_r = 0.5v_s$. Hence, considering positive numbers for $v(x)$, equation (1) can be simplified to

$$v(x) = (v_s - v_c)(0.5 - \pi^{-1}\arctan[(x-x_f)d^{-1}]) + v_c H(x_f - x). \quad (2)$$

To explore the sensitivity of our inversion algorithm to common mode fault-parallel reference frame errors, we conducted a range of tests with fault-parallel offsets of up to 4 mm/yr to the observed station velocities. Within the range considered, we can summarize the resulting changes in parameter estimates by the following approximation. A 1 mm/yr error in v_r causes changes of 1-1.2 mm/yr in v_s, of 1-1.5 km in d and of ~ 1 km in x_f. The standard deviations quoted for our observed velocities relative to Eurasia include common mode errors with respect to that reference frame. On the basis of our sensitivity tests and the observed small fault-orthogonal displacement rates (relative to Eurasia) of our stations far away from the fault trace in the central Sumatra basin we therefore expect reference frame errors to be sufficiently accounted for in the formal parameter uncertainty estimates.

For our least squares inversion we divide the survey region (excluding Banda Aceh) into six SFS-orthogonal segments (Figure 1). Corresponding model slip rate profiles are presented in Figure 7. When we determine the three fault parameters for each of the six lines, the estimated fault location (x_f) is systematically displaced westward toward the trench from the mapped geological location of the fault. This offset is significant for the three northern traverses and indicates that within the adopted reference frame, displacement is not symmetrically distributed about the SF geologic trace. Fault-parallel strain is greater westward of the fault trace. Our sparse station distribution in the forearc ridge and forearc basin makes it impossible to identify any active offshore strike-slip faults with slip rates <10 mm/yr. To explore the range of potential offshore shear, we adopted a model that assumes all slip to be located on two partially locked dislocation surfaces, one on the SF, the other in the forearc basin, about 120-140 km away from the SF. We impose offshore slip at shallow depths in increments of 1 mm/yr and invert for SF parameters. Without a general change in the weighted RMS misfit, the offset in fault origin is reduced by several kilometers if we consider as much as 5 mm/yr of slip to occur offshore.

We obtain similar fault parameter estimates if we attribute part of the fault-parallel deformation in the forearc to oblique thrusting at the trench. The sparse station distribution in the forearc does not warrant a simultaneous inversion for SF and trench parameters. Similar to the case of additional strike-slip offshore, we employ a forward model to estimate the fault-parallel deformation due to oblique slip at the trench, using *Okada's* [1985] equations for dip-slip faults and the same trench geometry as *Prawirodirdjo et al.* [1997]. A high coupling coefficient [*Prawirodirdjo et al.*, 1997] of 1.0 at the southern part and of 0.8 at the northern part of the shallow (0-25 km) segments of the subduction surface yields trench-parallel deformation across the forearc equivalent to 3-5 mm/yr of strike slip for oblique convergence at angles up to 20° and at an average SF slip rate of 24 mm/yr. Tests with synthetic data reveal that for the given station distribution in the forearc, the three-parameter SFS inversion cannot distinguish between additional forearc deformation due to oblique slip at the trench and additional strike slip in the forearc basin.

Table 3 and Figure 7 summarize our inversion results. The range of modeled SF fault strike (N31°W to N39°W) has little impact on parameter estimates and RMS misfit, so we use N35°W as the average fault strike. RMS misfit for all profiles remains essentially unchanged if we include up to 4 mm/yr of fault creep into our inversion model. However, we did not find any geologic evidence of fault creep or corresponding references in the literature.

8. Modeling Results

The GPS-derived estimates of total slip rate and corresponding uncertainty are highly uniform along the entire fault length considered. They agree to within 5 mm/yr with independent estimates of forearc trench-parallel velocity calculated from slip vectors of thrust earthquakes. Depending on the model of Australia-Eurasia plate convergence pole of rotation employed, *McCaffrey et al.* [this issue] arrive at rates

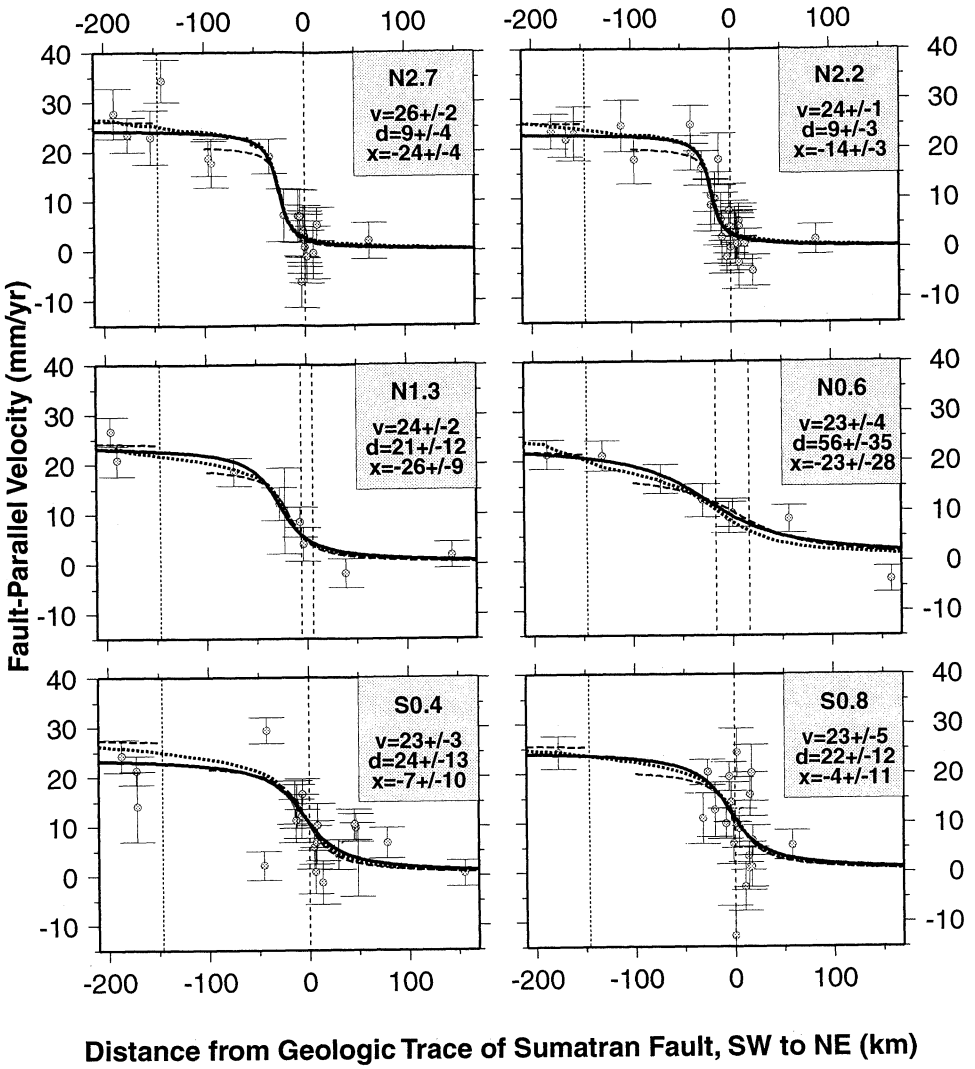

Figure 7. Fault-parallel components (circles) of GPS-measured displacement rates with associated formal one standard deviations as a function of orthogonal fault distance for six arrays of GPS sites that traverse the SF at different mean latitudes (indicated in the top right corner of each panel). Slip rate profiles of the best fitting (in a least squares sense) locked, vertical strike-slip fault models are shown as solid lines for a single dislocation surface and as dashed lines if additional shear of 5 mm/yr is considered offshore between 125 and 150 km southwest of the SF trace. Dotted lines include modeling of forearc deformation due to oblique subduction at the trench. Fault model parameters corresponding to the solid lines are shown as inserts; v (mm/yr) is the total (far field) slip rate, d (km) the locking depth, and x (km) the offset from the SF. The dotted vertical line near –150 km marks the approximate location of the Mentawai fault. At 1.3°N and 0.6°N the SFS consists of two major strands whose location with respect to the common reference position is indicated by parallel vertical dashed lines.

of 20±3 or 23±1 mm/yr for our segments south of the equator, of 27±7 or 29±3 mm/yr for the two central segments, and of 28±1 or 29±2 mm/yr for the Lake Toba segments. Our inferred slip rates of 26±2 mm/yr in the Lake Toba region (Figure 3) are only insignificantly higher than near the equator (23±3 mm/yr). At 2.2°N (Dolok Sanggul) our modeling places the fault plane 14±3 km west of the trace of the Renun segment [*Aldiss et al.*, 1983]. At 2.7°N (Sidikalang) the offset is 24±4 km. Near the Sidikalang array the geologic trace is associated with a pronounced linear structural low in the welded Toba Tuff. Along the Dolok Sanggul array, 70 km to the southeast, however, the main fault trace is topographically less prominent. Our simple model provides a good fit (Table 3) to the geodetic measurements in this area, although the single, locked, model fault plane is substantially offset westward from the geologic fault trace [*Sieh and Natawidjaja*, this issue].

Our modeling results for locking depth and fault location, however, show large (although not necessarily statistically significant) changes between different segments. These apparent variations are partially due to heterogeneous near-fault site distribution patterns. Our two central segments consist of only regional sites and lack dense fault-crossing arrays. Nevertheless, parameter and uncertainty estimates near 1.3°N are in good agreement with those for the two southern sections. However, just north of the equator, near 0.6°N, site coverage

Table 3. GPS-Derived Estimates of Sumatran Fault Slip Rates

Latitude	Number of Sites	Slip Rate, mm/yr	Slip Rate[a], mm/yr	Slip Rate[b], mm/yr	Locking Depth, km	Fault Plane[a] Offset, km	RMS Error, mm/yr
0.8°S	16	23±5	20±4	21±4	22±12	2±10	5
0.4°S	20	23±3	22±3	23±3	24±13	-4±8	5
0.6°N	8	23±4	19±3	20±4	56±35	7±26	4
1.3°N	9	24±2	20±2	22±2	21±12	-17±6	3
2.2°N	27	24±1	21±1	23±1	9±3	-14±3	4
2.7°N	19	26±2	23±1	25±2	9±4	-24±4	4
5.5°N	14	<13[c]			<16		

These modeling results assume no fault creep and are based on site velocities relative to Eurasia.
[a]Additional shear of 5 mm/yr is considered due to strike slip in the forearc offshore region.
[b]Additional shear in the forearc offshore region is considered due to oblique convergence at the trench.
[c]Fault plane intersects array and locking depth does not exceed specified limit.

is sparse, and we obtain rather poor estimates (standard deviations exceed 25 km, Table 3) of locking depth and fault location.

Although the fault-parallel velocity profiles at 2.2°N and 2.7°N (Figure 3) do not specifically exclude right-lateral slip of several millimeters per year within the southwestern margins of the Bukit Barisan (Sipakpahi-Kluet fault zone [*Aldiss et al.*, 1983]), such deformation could not account for the observed offset between the geomorphic fault trace of the Renun segment and the model fault plane. Location of the latter is largely controlled by the observed displacement of sites close to the SF. A fault plane dipping to the southwest would cause an apparent offset in model estimates of fault location since our model assumes a vertical surface. Dip angles of focal solutions of nearby recent earthquakes show no significant deviation from the vertical. The observed offset may point to active faulting along subparallel strands to the west or reflect heterogeneity in the elastic properties of the upper crust. Creep at or within 500 m of the geologic fault trace is <3 mm/yr for both array-crossing locations.

Near 1°N, the SF splays into two prominent branches (Figure 4). Our least squares inversion of the observed displacement in the two central segments yields a solution for the single vertical fault plane that is positioned between the two fault branches. The model fault, however, is closer to the (western) Angkola segment, indicating that slip is less on the (eastern) Barumun segment.

Since two of our geodetic sites (P051 and P37E) are located between these bifurcating fault segments, we can estimate the distribution of slip from a superposition of our screw dislocation model. We assume that slip is confined to the two geologic fault traces with locking depths in the range of 10-20 km as our other single fault plane solutions suggest. Given the estimated total slip rate at that latitude (23 mm/yr, Table 3) and the fault-parallel velocity component (9±3 mm/yr) measured at P37E (located 18 km away from the eastern and 15 km away from the western branch), we can solve for slip rates on both fault segments (2-4 mm/yr for the eastern, 19-21 mm/yr for the western branch). At 0.9°N the site P051 is located almost halfway between the two fault strands (orthogonal distances of 13 and 14 km, respectively). The measured fault-parallel displacement rate of 4±4 mm/yr appears to be quite low, since it not only requires that essentially all of the slip is located on the Angkola segment but also places an upper limit of 7 km on the locking depth in order to arrive at a solution. Stream offsets [*Sieh and Natawidjaja*, this issue] and seismicity confirm an active Angkola segment. The 1892 Tapanuli earthquake (Figure 4) resulted in right-lateral displacement of several meters as measured by triangulation across this fault zone (1.9 m reported by *Rock et al.* [1983], based on work by *Müller* [1895]; 4.5±0.7 m estimated by *Prawirodirdjo et al.* [this issue]).

9. Discussion

Displacement of Sumatra's western coast with respect to the basin, measured with GPS across the SFS at a perpendicular distance of ~ 200 km, averages 21±5 mm/yr in the direction of SF strike N35±8°W for almost 400 km of fault trace (0.6°S to 2.7°N). Modeling of the GPS-derived velocity field is consistent with the notion that most of this deformation is due to right-lateral slip on the SF. Allocating up to 5 mm/yr of slip offshore, however, yields a better match of geologic and GPS-derived fault locations. The Mentawai fault [*Diament et al.*, 1992] falls within the range of possible locations for this offshore motion. *Sieh and Natawidjaja* [this issue] postulate, however, that the Mentawai fault has become inactive, perhaps in the past 100 kyr, and thus is unlikely to accommodate present day right-lateral slip. We prefer to attribute the inferred additional shear to interseismic elastic strain accumulation due to stress increase on the subduction thrust fault [*Prawirodirdjo et al.*, 1997]. Furthermore, the rotation of forearc slip vectors suggests that the remaining part of the arc-parallel component of Australia-Eurasia plate convergence occurs beyond the trench side margin of our geodetic array, that is, between the forearc islands and the trench [*McCaffrey et al.*, this issue].

Fault-parallel deformation rates for the different tectonic regions (forearc ridge, coastal margins, near fault areas, back arc basin) only slightly increase northward. They account for 7.7±5.2 x 10^{-8}yr^{-1} of stretching at an azimuth of N39°W for the northwestern part of our geodetic network. This rate agrees with the early uniform strain rate estimate of 3-4 x 10^{-8}yr^{-1} [*McCaffrey*, 1991] and is close to *McCaffrey's* [1996] refined arc-parallel extensional strain rate of 1.7±0.4 x 10^{-8}yr^{-1} derived for the forearc from slip vector deflections of thrust earthquakes. We calculate a geodetic strain rate for the eastern basin at less than 10^{-8}yr^{-1}. Here we do not see evi-

Table 4. GPS-Derived SF Fault-Normal Average Displacement Rates Relative to Eurasia

Latitude	Forearc Ridge	Forearc Basin	SW of of SF	NE of of SF	Back-Arc Basin
0.8°S	36±4		12±5	10±8	9±4
0.4°S	33±10		18±7	11±8	10±3
0.6°N	20±4	3±4	2±2	7±7	4±3
1.3°N	9±3		7±4	6±4	6±3
2.2°N	22±3	7±10	12±2	11±2	4±3
2.7°N	17±5	13±4	10±4	8±2	8±4
5.5°N[a]			-2±8[b]	-5±2[c]	0±6[d]

Displacement rates (in mm/yr) are averaged for the different fault segments (indicated by their approximate latitude, see Figure 1) from displacement rates of sites located on the Mentawai Islands (forearc ridge), between the Mentawai fault and the Sumatran coast (forearc basin), onshore southwest of the SF, in the Bukit Barisan mountains northeast of the SF, and in the eastern Sumatran lowlands (back arc basin). Rates are fault-normal for an average strike of N35°W, except at 5.5°N latitude where the average strike of the Seulimeum segment is N31°W.

[a]Rates are relative to the easternmost site of the array (K501, Table 2).

[b]Sites are southwest of the Aceh segment.

[c]Sites are between the Aceh and Seulimeum segments.

[d]Single site is east of the Seulimeum segment.

dence for the back arc contraction suggested by *Bellier and Sébrier* [1995].

Within our level of geodetic precision, fault-normal displacement rates change little along the onshore segments (columns labeled southwest of SF, northeast of SF, and back arc basin in Table 4) of all but one array (2.2°N). In particular, we do not detect any significant change across the SF, that is, fault motion appears to be strictly strike slip. At 2.2°N, however, the transect sites move toward the back arc basin at a fault-orthogonal rate of 7±4 mm/yr, equivalent to a compressional strain rate across the southeastern part of the Batak tumor of 11±6 x 10^{-8}yr^{-1}. This deformation appears to be unrelated to the change in SFS strike by 7±3° near Tarutung (2.0°N). A slip rate of 24±1 mm/yr (Table 3) would produce a fault-orthogonal expansion rate of only 3±1 mm/yr, which is small compared to the opening rate of the Tarutung valley due to the 3-km-wide dilatational step over [*Sieh and Natawidjaja*, this issue].

The Aceh and the Seulimeum segments (Figure 2) are recognized as the northernmost segments of the SF. Our geodetic measurements allow little right-lateral slip on the Aceh segment. This observation is consistent with data from multichannel acoustic offshore surveys (J. Curray, oral communication, 1999) and onshore geologic field work [*Sieh and Natawidjaja*, this issue] that consider this branch to be presently inactive and identify the Seulimeum segment as the currently active branch. Applying reasonable limits to the locking depth, slip on the Seulimeum segment at the location of our geodetic array, however, is at most 13 mm/yr (Table 3). This branch is located close to significant recent seismic activity (offshore, 1985, M_w=5.3, centroid moment tensor (CMT); onshore, 1975, M_s=6.2, Preliminary Determination of Epicenters (PDE)). If major slip occurs onshore it must be confined to the coastal margins beyond the end points of our geodetic array.

The geologic structure of the coastal region to the south [*Bennett et al.*, 1981b] does not include any NW-trending onshore strike-slip faulting. Although the Tapaktuan fault, the southwest offshore continuation of the Batee fault, is considered active [*Cameron et al.*, 1982], it cannot account for the apparent slip deficit because the Batee fault branches off the SFS's Aceh segment well southeast of the array. However, two north trending splays of the SFS ~ 100 km and 180 km east of our array may account for significant dextral slip. The subparallel Lhokseumawe and Samalanga Sipopok faults (Figure 1) reach the strait of Malacca at 97.2°E and 96.4°E, respectively. Both faults are considered active since at least the late Oligocene [*Keats et al.*, 1981]. The Samalanga Sipopok fault can be traced to the central part of the Barisan Mountains near the origin of the Batee fault [*Cameron et al.*, 1983], whereas farther southeast the Lhokseumawe fault defines the eastern boundary of the mountain range [*Keats et al.*, 1981]. However, there is currently no evidence for any offshore link of either of these subparallel faults to strike-slip structures in the Andaman Sea (J. Curray, oral communication, 1999). Thus the geodetic slip rates estimated at the northern tip of Sumatra for the Aceh and Seulimeum segments indicate that additional GPS observations over a broader spatial region will be required to determine the slip deficit.

To estimate the seismic potential associated with strain accumulation at the fault, we employ a simple model that relates coseismic slip (u), locking depth (d), rigidity (μ), and rupture length (l) to seismic moment (M_0) [*Aki and Richards*, 1980]

$$M_0 = u \mu l d. \quad (3)$$

With up to 4 mm/yr of creep, the minimum slip deficit along

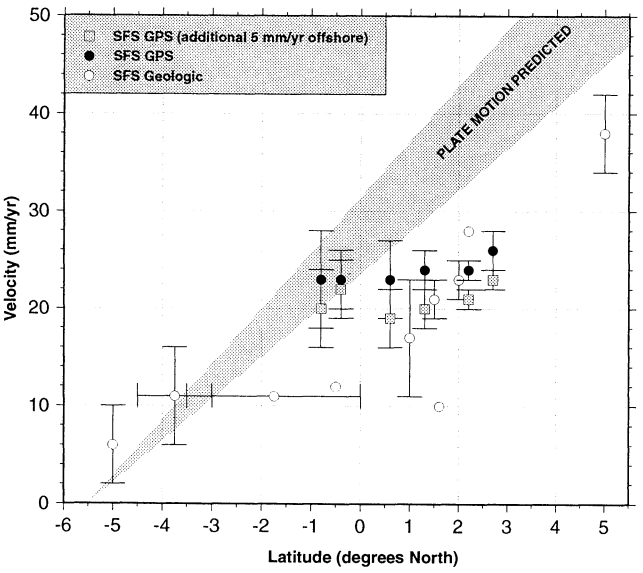

Figure 8. Northward increase of Sumatran fault slip rates. Geologic estimates include those of Table 1 and of *Bellier and Sébrier* [1995]; geodetic rates are based on the best fitting models shown in Figure 7 and listed in Table 3. The shaded area labeled "plate motion predicted" corresponds to the rate of trench-parallel forearc motion relative to the Sunda Shelf predicted from a three-plate (Australia, forearc, southeast Asia) uniform strain rate model [*McCaffrey*, 1991].

Table 5. Onshore SF-Parallel GPS-Derived Velocities

Latitude[a]	SW Site Code	Site Distance to SF[b], km	Velocity [c], mm/yr	NE Site Code	Site Distance to SF[b], km	Velocity[c], mm/yr	SW-NE Velocity[d], mm/yr
0.8°S	PADA	-27	20±3	P015	58	5±3	15±4
0.4°S	TANJ	-42	29±3	PAUH	78	6±3	23±4
0.6°N	AIRB	-72	16±3	PASI	57	8±3	8±4
1.3°N	SIKA	-74	18±3	BINA	39	-2±3	20±4
2.2°N	PAND	-36	25±4	DEMU	88	2±3	23±4
2.7°N	JULU	-31	20±3	DSIM	65	3±4	17±4

[a]Approximate location of fault-crossing line is indicated.
[b]Orthogonal distance to geologic fault trace is given; positive numbers indicate locations northeast of fault.
[c]SF-parallel site velocity component is given relative to Eurasia for an average fault strike of N35°W.
[d]SF-parallel velocity is given of site located southwest of fault relative to site northeast of fault.

the fault segments covered by our network is 19 mm/yr. At a locking depth of 15 km, a crustal rigidity of 4×10^{10} N/m^2, and a rupture length of 40 km, 19 mm of seismic slip yields a corresponding moment of 4.6×10^{17} N m or, after conversion to moment magnitude [*Hanks and Kanamori*, 1979], M_w=5.7. Annual strain accumulation along the 400 km segment of the fault is therefore equivalent to more than 10 M_w=5.7 events. In connection with the empirically derived recurrence intervals, this estimate confirms a significant seismic moment deficit of the SFS on decadal timescales.

Finally, further field work may be required to resolve a significant discrepancy between GPS-derived slip rates and geologic rates (Figure 8). Although GPS and geologic slip rate estimates agree north of the equator, geodetically determined slip rates of 23 mm/yr are higher by ~ 10 mm/yr than the geologic estimates between the equator and 1°S. *Sieh and Natawidjaja* [this issue, Plate 4c] propose that the SF is composed of northern and southern domains slipping at rates of 25 and 10 mm/yr, respectively, linked by a central transpressional domain around the equator, deforming at 15 mm/yr. This rate of the transtension of the forearc sliver at the equator is close to our geodetic rate for the Angkola branch of the Equatorial Bifurcation. One could argue that the Angkola branch is a part of this transtensional regime, hence the apparent strike-slip rate of 15 mm/yr.

Still, the inferred geodetic rate of 23 mm/yr south of the equator does not support *Sieh and Natawidjaja*'s [this issue] model. We acknowledge that the rates obtained from our inversion are largely constrained by vectors located on the forearc islands. This holds for the Bukittinggi transect where very large formal uncertainties render the fault parameter estimates useless when we exclude the forearc sites. For the Solok transect, however, we obtain a consistent estimate of v_s=21±7 mm/yr, x_f=0±14 km, and d=17±13 km even if we limit the fault-orthogonal distance of sites considered in the inversion to 40 km. Two sites on the west coast of Sumatra (P002 and TOBO, see Figure 5) have velocities higher than 3 cm/yr, but these velocities are so extreme that they do not fit the curves shown on Figure 7. Neither site is included in any of our parameter estimates. We cannot resolve how the motion is distributed across the forearc with our geodetic data, and we cannot properly determine a slip rate on the SF without including data from the forearc islands.

Our site distribution, however, permits us to compare onshore displacement rates at various latitudes (Table 5). With the exception of a low value for AIRB-PASI, all five other considered station pairs show fault-parallel relative velocities of 15-23 mm/yr. The displacement rates are uncorrelated with latitude. Since the subduction seismogenic zone reaches nearly to the SF, it is possible that the observed relative velocities between site pairs are affected by margin-parallel strain due to oblique subduction. The analysis of GPS-derived forearc strain and slip vector orientation patterns, however, suggests that most of the non-SF related sources of fault-parallel deformation are located trenchward of the forearc islands [*McCaffrey et al.*, this issue]. Hence we can infer that almost all of the onshore displacement observed is due to slip on the SF or nearby subparallel faults. Within the framework of our single surface dislocation model we can then regard the relative site velocities listed in Table 5 as lower bounds for the SF slip rate at the corresponding latitude. Averaging the results of the two southernmost lines yields a minimum rate of 19±6 mm/yr for SF slip in the Minangkabau area. This lower limit corroborates our model estimates obtained from site velocities that include locations on the Mentawai Islands.

If both our rates and the model proposed by *Sieh and Natawidjaja* [this issue] are correct, then there must be significant shear on the forearc between the SF and the forearc islands. Recent published results of a GPS geodetic survey [*Duquesnoy et al.*, 1999] in the Lake Singkarak area indicate 27.5±2.5 mm/yr of fault-parallel motion for two sites located near Sumatra's west coast with respect to a reference point 30 km east of the SF. These results support our inferred SF slip rates at that latitude. Resolving the apparent discrepancy between the geodetic and geologic slip rates south of the equator may require additional GPS measurements by lengthening the time span of our data, and perhaps extending our network southward to include new sites between the coast and the SF.

10. Conclusions

Geodetic measurements from GPS regional surveys in west and north Sumatra and from annual occupations of five SF-crossing small-aperture arrays in 1990-1996 outline the surface deformation field of this seismically active segment of the Australian-Eurasian plate margin. Nearly all onshore deformation can be attributed to right-lateral slip at the Sumatran fault. Between 1°S and the equator, geodetically deter-

mined slip rates of 23 mm/yr are higher than geologic estimates. They increase insignificantly to 26 mm/yr at 2.7°N and match geologic rates between 1°N and 3°N. Although RMS misfit remains essentially unchanged if ~ 5 mm/yr of the overall slip occurs in the forearc in the offshore region, reductions of apparent westward offsets in modeled SF trace support this scenario. Locking depths on the fault are estimated at 10-20 km, except where the SF trace splays to two branches north of the equator. Fault creep may account for a small fraction of total slip. With part of the total fault-parallel deformation attributed to offshore sources, modeled fault locations generally agree with geologically identified fault traces. Near Toba caldera, modeled slip is focused several kilometers west of the geologic fault plane.

The SFS separates the eastern basin, a region that is part of the Sunda Shelf and undergoes little internal deformation, from the western coastal areas of the forearc sliver. The northern sections of the forearc are subject to stretching and may accommodate fault-parallel deformation due to oblique thrusting at the trench.

Acknowledgments. We are indebted to Jakub Rais, Director of the National Coordination Agency for Surveying and Mapping, for his encouragement and support of our work since its inception, and to his deputy and later director, Paul Suharto, who passed away in 1999. Site monumentation and data collection for this study could only have been accomplished with the help of many Indonesian, U.S., and Japanese surveyors. A list of these individuals is given by *Prawirodirdjo et al.* [this issue]. We are grateful to James Stowell and his staff at the UNAVCO Boulder facility (Bruce Stephens, Mike Jackson) for training and providing field engineers, to Joe Bearden from Caltex for logistical support and providing GPS receivers for surveys in the backarc basin, and to Klass Villanueva and Joenil Kahar from ITB for their assistance. Ken Alexander, Fritz Brunner, Martin Hendy, John Manning, and Paul Tregoning made Australian tracking data available; Miranda Chin and Gerry Mader furnished CIGNET data. We thank Eric Calais, Paul Tregoning, and Peter Zwick for their assistance in data collection and analysis, Peng Fang of the Scripps Orbit and Permanent Array Center for supplying precise satellite ephemerides and global GPS solutions, and colleagues from the International GPS Service for global tracking data since 1992. Kerry Sieh and Danny Natawidjaja generously provided an advanced copy of their detailed map of the Sumatran fault geologic trace and helpful comments on the manuscript. Reviews by Richard Bennett and Jeff Freymueller are greatly appreciated. Figures were drawn with GMT [*Wessel and Smith*, 1991]. Supported at SIO by NSF grants EAR-8817067 and EAR-9004376 and NASA grant NAGW-2641, at RPI by NSF grants EAR-8908759 and EAR-9114349, and by the Indonesian government.

References

Aki, K., and P. G. Richards, *Quantitative Seismology: Theory and Methods*, W. H. Freeman, New York, 1980.

Aldiss, D. T., R. Whandoyo, A. G. Sjaefudien, and Kusjono, The geology of the Sidikalang quadrangle, Sumatra, report, Geol. Res. and Dev. Cent., Bandung, Indonesia, 1983.

Argus, D. F., and R. G. Gordon, No-net-rotation model of current plate velocities incorporating plate motion model NUVEL-1, *Geophys. Res. Lett., 18*, 2039-2042, 1991.

Bellier, O., and M. Sébrier, Is the slip rate variation on the Great Sumatran fault accommodated by fore-arc stretching?, *Geophys. Res. Lett., 22*, 1969-1972, 1995.

Bellier, O., M. Sébrier, S. Pramumijoyo, T. Beaudouin, H. Harjono, I. Bahar, and O. Forni, Paleoseismicity and seismic hazard along the Great Sumatran fault (Indonesia), *J. Geod., 24*, 169-183, 1997.

Bennett, J. D., et al., Geologic map of the Banda Aceh quadrangle, north Sumatra, Geol. Res. and Dev. Cent., Bandung, Indonesia, 1981a.

Bennett, J. D., et al., The geology of the Calang quadrangle, Sumatra, Geol. Res. and Dev. Cent., Bandung, Indonesia, 1981b.

Beutler, G., P. Morgan, and R. E. Neilan, International GPS Service for Geodynamics: Tracking satellites to monitor global change, *GPS World, 4*(2), 40-46, 1993.

Bock, Y., Medium distance GPS measurements, in *GPS for Geodesy, Lect. Notes Earth Sci.*, vol. 60, 2nd ed., edited by P. J. G. Teunissen and A. Kleusberg, pp. 483-536, Springer-Verlag, New York, 1998.

Bock, Y., R. McCaffrey, J. Rais, and I. Murata, Geodetic studies of oblique plate convergence in Sumatra, *Eos Trans. AGU, 71*, 857, 1990.

Cameron, N. R., et al., The geology of the Tapaktuan quadrangle, Sumatra, report, Geol. Res. and Dev. Cent., Bandung, Indonesia, 1982.

Cameron, N. R., et al., The geology of the Takengon quadrangle, Sumatra, report, Geol. Res. and Dev. Cent., Bandung, Indonesia, 1983.

Chesner, C. A., W. I. Rose, A. Deino, R. Drake, and J. A. Westgate, Eruptive history of Earth's largest Quaternary caldera (Toba, Indonesia) clarified, *Geology, 19*, 200-203, 1991.

DeMets, C., R. G. Gordon, D. F. Argus, and S. Stein, Effects of recent revisions to the geomagnetic reversal time scale on estimates of current plate motions, *Geophys. Res. Lett., 21*, 2191-2194, 1994.

Diament, M., H. Harjono, K. Karta, C. Deplus, D. Dahrin, M. T. Zen, M. Gérard, O. Lassal, A. Martin, and J. Malod, Mentawai fault zone off Sumatra: A new key to the geodynamics of western Indonesia, *Geology, 20*, 259-262, 1992.

Dowdy, S., and S. Wearden, *Statistics for Research*, 2nd ed., John Wiley, New York, 1991.

Duquesnoy, T., O. Bellier, M. Sébrier, M. Kasser, C. Vigny, F. Ego, I. Bahar, E. Putranto, and I. Effendi, Etude géodésique d'un segment sismique de la Grande Faille de Sumatra (Indonésie), *Bull. Soc. Géol. Fr., 170*, 25-30, 1999.

Dziewonski, A. M., T.-A. Chou, and J. H. Woodhouse, Determination of earthquake source parameters from waveform data for studies of global and regional seismicity, *J. Geophys. Res., 86*, 2825-2852, 1981.

Fang, P., and Y. Bock, Scripps Orbit and Permanent Array Center report to the IGS –1995, in *1994 Annual Report, International GPS Service for Geodynamics*, edited by J. F. Zumberge, R. Liu and R. E. Neilan, pp. 213-233, IGS Cent. Bur., Jet Propul. Lab., Pasadena, Calif., 1995.

Fang, P., and Y. Bock, Scripps Orbit and Permanent Array Center 1995 report to IGS in *International GPS Service for Geodynamics 1995 Annual Report*, edited by J. F. Zumberge, M. P. Urban, R. Liu, and R. E. Neilan, pp. 103-124, IGS Cent. Bur., Jet Propul. Lab., Pasadena, Calif., 1996.

Fauzi, R. McCaffrey, D. Wark, Sunarjo, and P. Y. Haryadi, Lateral variation in slab orientation beneath Toba caldera, northern Sumatra, *Geophys. Res. Lett., 23*, 443-446, 1996.

Feigl, K. L., R. W. King, T. A. Herring, and M. Rothacher, A scheme for reducing the effect of selective availability on precise GPS carrier phase measurements, *Geophys. Res. Lett., 18*, 1289-1292, 1991.

Fitch, T. J., Plate convergence, transcurrent faults and internal deformation adjacent to southeast Asia and the western Pacific, *J. Geophys. Res., 77*, 4432-4460, 1972.

Genrich, J. F., Y. Bock, R. McCaffrey, E. Calais, C. W. Stevens, and C. Subarya, Accretion of the southern Banda arc to the Australian plate margin determined by Global Positioning System measurements, *Tectonics, 15*, 288-295, 1996.

Hamilton, W., Tectonics of the Indonesian Region, *U.S. Geol. Surv. Prof. Pap., 1078*, 1979.

Hanks, T. C., and H. Kanamori, A moment magnitude scale, *J. Geophys. Res., 84*, 2348-2350, 1979.

Hartley, H. O., The modified Gauss-Newton method for the fitting of non-linear regression functions by least squares, *Technometrics, 3*, 269-280, 1961.

Herring, T. A., Global Kalman filter VLBI and GPS analysis program (GLOBK) version 4.1, Massachusetts Institute of Technology, Cambridge, 1997.

Katili, J. A., and F. Hehuwat, On the occurrence of large transcurrent faults in Sumatra, Indonesia, *J. Geosci., Osaka City Univ., 10*, 5-17, 1967.

Keats, W., et al., The geology of the Lhokseumawe quadrangle, report, Geol. Res. and Dev. Cent., Bandung, Indonesia, 1981.

McCaffrey, R., Slip vectors and stretching of the Sumatran forearc, *Geology, 19*, 881-884, 1991.

McCaffrey, R., Estimates of modern arc-parallel strain rates in fore arcs, *Geology, 24*, 27-30, 1996.

McCaffrey, R., Y. Bock, and J. Rais, Crustal deformation and oblique plate convergence in Sumatra, *Eos Trans. AGU, 71*, 637, 1990.

McCaffrey, R., P. Zwick, Y. Bock, L. Prawirodirdjo, J. Genrich, C. W. Stevens, S. S. O. Puntodewo, and C. Subarya, Strain partitioning during oblique plate convergence in northern Sumatra: Geodetic and seismologic constraints and numerical modeling, *J. Geophys. Res.*, this issue.

Müller, J., Nota betreffende de verplaatsing van eenige triangulatie pilaren in de residentie Tapanoeli tgv de aardbeving van 17 Mei 1892, *Natuurwet. Tijdschr. Ned. Indie, 54*, 299-307, 1895.

Natawidjaja, D. H., and K. Sieh, Slip-rate along the Sumatran transcurrent fault and its tectonic significance, paper presented at conference on Tectonic Evolution of Southeast Asia, Geol. Soc. London, Dec. 7-8, 1994.

Newcomb, K. R., and W. R. McCann, Seismic history and seismotectonics of the Sunda arc, *J. Geophys. Res., 92*, 421-439, 1987.

Okada, Y., Surface deformation due to shear and tensile faults in a half-space, *Bull. Seismol. Soc. Am., 75*, 1135-1154, 1985.

Page, B. G., J. D. Bennett, N. R. Cameron, D. Mc. C. Bridge, D. H. Jeffery, W. Keats, and J. Thaib, A review of the main structural and magmatic features of northern Sumatra, *J. Geol. Soc. London, 136*, 569-579, 1979.

Prawirodirdjo, L., et al., Geodetic observations of interseismic strain segmentation at the Sumatra subduction zone, *Geophys. Res. Lett., 24*, 2601-2604, 1997.

Prawirodirdjo, L., Y. Bock, J. F. Genrich, S. S. O. Puntodewo, J. Rais, C. Subarya, and S. Sutisna, One century of tectonic deformation along the Sumatran fault from triangulation and Global Positioning System surveys, *J. Geophys. Res.*, this issue.

Puntodewo, S. S. O., et al., GPS measurements of crustal deformation within the Pacific-Australia plate boundary zone in Irian Jaya, Indonesia, *Tectonophysics, 237*, 141-153, 1994.

Rock, N. M. S., D. T. Aldiss, J. A. Aspden, M. C. G. Clarke, A. Djunuddin, W. Kartawa, Miswar, S. J. Thompson, and R. Whandoyo, The geology of the Lubuksikaping quadrangle, Sumatra, report, 60 pp. and map, Geol. Res. and Dev. Cent., Bandung, Indonesia, 1983.

Savage, J. C., and R. O. Burford, Geodetic determination of relative plate motion in central California, *J. Geophys. Res., 78*, 832-845, 1973.

Sieh, K., and D. H. Natawidjaja, Neotectonics of the Sumatran fault, Indonesia, *J. Geophys. Res.*, this issue.

Sieh, K., J. Rais, and Y. Bock, Neotectonic and paleoseismic studies in west and north Sumatra, *Eos, Trans. AGU. 72*(44), Fall Meet. Suppl., 460, 1991.

Sieh, K., J. Zachariasen, Y. Bock, L. Edwards, F. Taylor, P. Gans, Active tectonics of Sumatra, *Geol. Soc. Am. Abstr. Programs, 26*, A-382, 1994.

Sillard, P., Z. Altamimi, and C. Boucher, The ITRF96 realization and its associated velocity field, *Geophys. Res. Lett., 25*, 3223-3226, 1998.

Smith, W. H. F., and D. T. Sandwell, Global seafloor topography from satellite altimetry and ship depth soundings, *Science, 277*, 1956-1962, 1997.

Stevens, C., R. McCaffrey, Y. Bock, J. Genrich, Endang, C. Subarya, S. S. O. Puntodewo, Fauzi, and C. Vigny, Rapid rotations about a vertical axis in a collisional setting revealed by the Palu fault, Sulawesi, Indonesia, *Geophys. Res. Lett., 26*, 2677-2680, 1999.

Sukmono, S., M. T. Zen, W. G. A. Kadir, L. Hendrajaya, D. Santoso, and J. Dubois, Fractal geometry of the Sumatra fault seismicity and its possible application to earthquake prediction, *Bull. Seismol. Soc. Am., 87*, 1685-1690, 1997.

Sun, J. C., and T. C. Pan, The probability of very large earthquakes in Sumatra, *Bull. Seismol. Soc. Am., 85*, 1226-1231, 1995.

Tregoning, P., F. K. Brunner, Y. Bock, S. S. O. Puntodewo, R. McCaffrey, J. F. Genrich, E. Calais, J. Rais, and C. Subarya, First geodetic measurement of convergence across the Java trench, *Geophys. Res. Lett., 21*, 2135-2138, 1994.

Van Bemmelen, R. W., *The Geology of Indonesia*, 2nd ed., Martinus Nijhoff, The Hague, Netherlands, 1970.

Wessel, P., and W. H .F. Smith, Free software helps map and display data, *Eos Trans. AGU., 72*, 441, 445-446, 1991.

Zachariasen, J., Paleoseismology and paleogeodesy of the Sumatran subduction zone: A study of vertical deformation using coral microatolls, Ph.D. thesis, Calif. Inst. of Technol., Pasadena, 1998.

Zachariasen, J., K. Sieh, F. W. Taylor, R. L. Edwards, and W. S. Hantoro, Submergence and uplift associated with the giant 1833 Sumatran subduction earthquake: Evidence from coral microatolls, *J. Geophys. Res., 104*, 895-919, 1999.

Zhang, J., Y. Bock, H. Johnson, P. Fang, J. Genrich, S. Williams, S. Wdowinski, and J. Behr, Southern California Permanent GPS Geodetic Array: Error analysis of daily position estimates and site velocities, *J. Geophys. Res., 102*, 18,035-18,055, 1997.

Zwick, P., and R. McCaffrey, Seismic slip rate and direction of the Great Sumatra fault based on earthquake fault plane solutions, *Eos Trans. AGU., 72*(17), Spring Meet. Suppl., 201, 1991.

Y. Bock, J. F. Genrich, and L. Prawirodirdjo, Cecil H. and Ida M. Green Institute of Geophysics and Planetary Physics, Scripps Institution of Oceanography, University of California, San Diego, 9500 Gilman Drive, La Jolla, CA 92093-0225. (jgenrich@ucsd.edu; ybock@ucsd.edu; linette@josh.ucsd.edu.)

R. McCaffrey and C. W. Stevens, Department of Earth and Environmental Sciences, Rensselaer Polytechnic Institute, Troy, NY 12180-3590. (mccafr@rpi.edu.)

S. S. O. Puntodewo and C. Subarya, BAKOSURTANAL, Jl. Raya Jakarta Bogor km 46, Cibinong, Bogor, Indonesia. (geodesi@server.indo.net.)

S. Wdowinski, Department of Geophysics and Planetary Sciences, Tel Aviv University, Ramat Aviv, Israel. (shimon@geo1.tau.ac.il.)

(Received May 17, 1999; revised October 26, 1999;
accepted December 17, 1999.)